INTERACTION OF A SPHERICAL PARTICLE WITH A CONFINED LIQUID FILM

Subhasish Mitra[a], Elham Doroodchi[a], Geoffrey M. Evans[a]*

Vishnu Pareek[b], Jyeshtharaj B. Joshi[c, d]

[a]Discipline of Chemical Engineering, School of Engineering,
University of Newcastle, Callaghan NSW 2308, Australia
[b]Department of Chemical Engineering, Curtin University, Perth, WA 6102, Australia
[c]Homi Bhabha National Institute, Anushaktinagar, Mumbai 400 094, India
[d]Department of Chemical Engineering, Institute of Chemical Technology,
Matunga, Mumbai 400 019, India

*Author for correspondence
E-mail: Geoffrey.Evans@newcastle.edu.au

ABSTRACT

This paper reports on the collision interaction between a confined liquid film (water) and an impacting hydrophilic glass particle of different diameters (1.1-2mm) and impact velocities (0.2-1 m/s). Depending on the impact Weber number (1.4-23.9) of the particles either complete capture of the particle inside the film or complete penetration through the film were observed. In the latter case a certain amount of liquid mass was found to adhere to the particle surface which again depended on the impact Weber number. A criterion was developed based on the energy balance approach to demarcate between these two regimes. Also, an analytical model was proposed to approximately determine the liquid mass attached to the particle. Computationally, a three dimensional CFD model was developed using the VOF approach and dynamic meshing technique which was found to be in good agreement with the experimentally observed dynamics in these two regimes.

INTRODUCTION

Proper understanding of interaction of particles with gas-liquid interface is the key to successful design of many process engineering applications specifically where a uniform coating of liquid film over the particle surface or heat and mass transfer during such interaction are of interest. Some of these applications include coating of particles; scrubbing of dust-laden gases; contacting of feed droplets and catalyst particles in the vaporization zone of fluidized catalytic cracking reactors [4]; coking of bitumen, spray drying [5], fabrication of ceramic reinforced metal composites [12], recovery of minerals by film flotation [8] and may more. In all these interactions two distinct types of gas-liquid interface can identified – planar interface and curved interface. A significant number of studies have been reported on the interactions of hydrophobic objects having shapes of sphere and cylinder on a large planar interface explaining the biological instances of insects walking on the water [6] and mineral separation applications using flotation [7,8]. The fate of the impacting object depends primarily on the relative magnitude of impact inertia to surface tension which results into interface penetration, bounce off, or oscillation at the interface.

Two different types of interactions are known to occur when a spherical particle interacts with a curved gas-liquid interface. These interactions are: (1) when a smaller droplet impacts upon a larger particle; and (2) when a smaller particle impacts upon a larger droplet. For the first case, the droplet may either stick, rebound or splash, depending on the relative velocities between the droplet and particle, physical properties of the droplet and the hydrophobicity of the particle surface [2,4,9]. The second case remains rather less explored. Few studies [3, 5,10,14] have been reported on particle interaction with a larger curved gas-liquid (droplet) interface, which is significant to many industrial processes. Possible interaction mechanisms between the particles and droplets may be divided into four categories. Firstly, a particle may collide with a droplet and rebound off the interface. Secondly, a particle may collide, partly penetrate the interface and attach itself to the interface with oscillatory motion. Thirdly, a particle may completely penetrate one interface but not exit the other interface and thus remain within the droplet. Fourthly, a particle may penetrate both interfaces and completely shoot through the droplet. Two more sub-categories of the fourth interaction process are known; namely: (1) where a bubble may be entrained in the droplet along with the particle; and (2) the droplet may be completely fragmented into multiple satellite droplets by the impact of the particle [3].

The first three types of interaction possibly occur in the lower Weber number regime whilst the fourth interaction occurs in the high Weber number regime. In the fourth case, a certain amount of liquid mass always gets entrained with the impacting particle—where quantification of the liquid mass is important for heat and mass transfer calculations. In all these cases the impact kinetic energy of the particle is dissipated in overcoming the resistance forces contributed by surface tension, buoyancy, fluid drag, and capillary pressure force. The outcome of the collision will be determined by ratio of all the resistive forces to the impact inertia of the particle.

Only a few studies have been reported when a smaller particle collides with a larger droplet; whilst numerous studies have been reported for smaller droplets impacting on a larger solid (usually planar) surface. This can be attributed to the challenging nature of the experiments involved to observe moving particles colliding with and penetrating moving droplets. To avoid this difficulty, in this study, a suspended liquid film having two interfaces was chosen rather than a moving droplet as the impact target for a colliding particle. The system was investigated experimentally to determine: (1) the conditions under which the particle was captured entirely within the film; and (2) the quantity of the entrained liquid film when the particle completely penetrated both films. A criterion was developed, based on an energy balance approach, which marked the transition between the two modes of interaction. Furthermore, three a dimensional CFD model was developed, using the multiphase volume of fluid (VOF) method combined with dynamic meshing algorithm, to simulate the interaction dynamics.

EXPERIMENTAL

The experimental apparatus is shown in Figure 1. Interaction characteristics were investigated experimentally for glass ballotini particles (Potter Mix, Australia) of different sizes in the range of 1.1-2.0 mm.
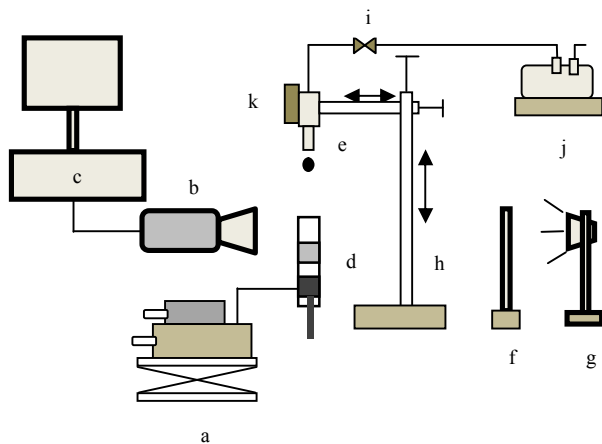
Figure 1 Schematic of experimental setup - a) X-Y optical traverse with height elevation jack b) high speed CCD camera c) computer d) capillary tube with piston holding the liquid film e) particle release nozzle f) diffuser screen g) light source h) particle release nozzle position varying mechanism i) solenoid valve j) vacuum pump k) laser source for alignment purpose.

Due to little irregularity in the particle diameter in such small range, several smaller sub-ranges were used with span of 0.1 mm, so that a mean of 0.05 mm was obtained to represent the uncertainty in particle size as $d_p \pm 0.05$ mm. A liquid film of pure (RO filtered) water was formed inside a transparent polymeric capillary tube of inner diameter 4.61mm. The tube was thoroughly cleaned with soap solution and acetone to remove any dirt before holding the film. To ensure consistency in the film thickness, the film was formed several times and the capillary tube was weighed before and after the film was formed to determine the film mass. The measured film mass was consistently obtained as 57 ± 3 mg leading to very consistent film thickness of 3.43 ± 0.16 mm. Since the capillary force is not sufficient by itself to support the liquid film of such mass, gradual descent of the film was prevented by applying upward pressure using a tightly sealed piston at the bottom of the capillary tube. The tube assembly was mounted on an X-Y optical traverse with micrometric precision. A particle release mechanism capable of sliding both in horizontal and vertical direction with millimetric precision was used to hold the particle at the tip of a stainless steel capillary nozzle (ID 0.03") by vacuum. A vacuum pump was connected to the nozzle via a solenoid valve. The particle release process was triggered by turning off the solenoid valve hence breaking the vacuum pull.

To ensure the particle fall was consistent, a separate experiment was carried out by dropping the particle several times from the same position. The alignment of the particle release nozzle with the capillary tube below was undertaken using a low power (<5mW) laser source ensuring that the laser beam always pointed towards the centre of the tube before the particle was dropped. The impact velocity of the particle was varied in the experiment by changing the position of the particle release nozzle in the vertical direction. In those cases, where the particle completely penetrated the liquid film and settled at bottom of the tube, the remaining film above was carefully absorbed in a wick and the final film weight was determined by measuring mass difference of the wet and dry wick. Mass of liquid adhered to the particle then was determined by subtracting the weight of final film from the initially weighed film. Each experiment for each size range of particle was repeated at least 5 times for five different impact velocities. A backlighting imaging technique was used obtain good contrast images in shadowgraphy mode by placing a diffuser screen in front of a halogen light source (12V, 50W). A high speed camera (Phantom, v311, Vision Research, USA) was used to capture images at 1953 frame per second and 35 μs exposure time of the interaction process in a field of view (FOV) of 512 X 800 pixels.

IMAGE PROCESSING

Image processing was carried out to extract data of particle positions from images taken at different time instances. The particle boundary was tracked based on difference in pixel intensity relative to the background. Due to inconsistency in the pixel intensity in the images, first the pixel counts over the grayscale values (0-256) were made uniform by manipulating the image histogram. Figure 2a and 2b present the distribution of pixel counts over the entire grayscale and clearly indicates

the improvement obtained in the pixel uniformity after image processing. Next, the particle boundary was marked (Figure 2c) based on intensity difference between particle boundary and background and a user-defined range of possible particle radius. A circle was fitted to the particle thus identified and equivalent spherical radius and centroid data were obtained. These data were used in all subsequent calculations. All image processing was performed using an in-house MATLAB (*v: R2012b*) code.
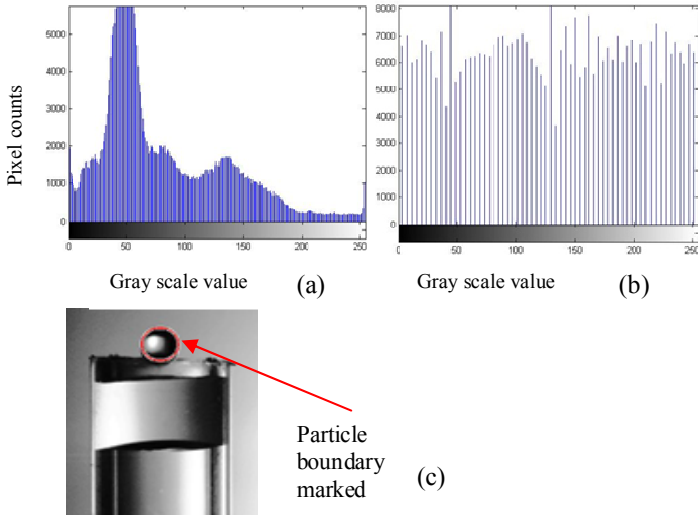

Figure 2 Image processing carried out showing a) pixel intensity distribution of raw image b) uniform pixel intensity distribution obtained after processing c) particle identified and a circle is fitted.

PARTICLE-LIQUID FILM INTERACTION OUTCOMES

When a particle impinges on a liquid film the interaction outcomes depend on the impact kinetic energy and the various resistive forces encountered in the liquid film. At smaller impact kinetic energy these resistive forces dominate and the particle may either be captured at the top interface or penetrate the top interface and retained at the bottom interface. At higher Weber number the particle has sufficient kinetic energy to overcome the resistive forces met in the liquid film and completely penetrate both interfaces.

A schematic of the process indicating the geometry and forces is presented in Figure 3. Consider a particle of diameter, d_p, of density, ρ_p, impacts on a liquid film of thickness, l_f, with velocity, v_p. The interface deforms as the particle moves downward and a three phase contact line of radius, r_{tpcl}, forms on the particle surface. Submergence of the particle is denoted by the penetration angle, β, which varies from 0 to 180° denoting zero to complete penetration. Contact angle, θ, is obtained by drawing two tangents at the interface and at point of contact on particle surface. Polar angle, ψ, at the particle centre obtained by subtracting β from θ. Various forces i.e. gravity, drag, buoyancy and capillary force act on the particle and resultant force decelerate its motion.
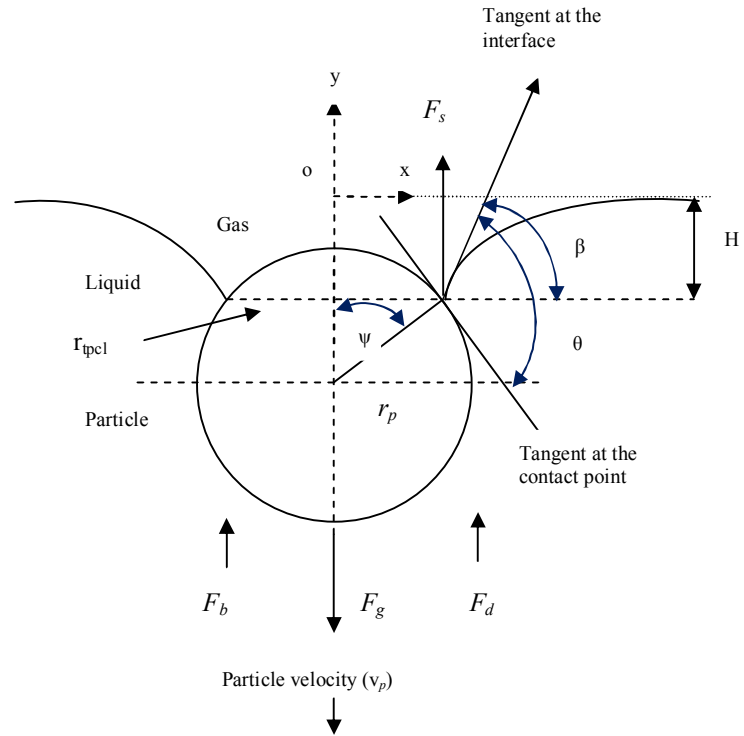
Figure 3 Schematic of various forces acting on the particle during penetration of the liquid film [8,11]

Kinetic energy of the impacting particle is obtained as:

$$E_{k0} = \frac{1}{2}\left(\frac{\pi}{6}d_p^3\rho_p\right)v_p^2 \qquad (1)$$

When particle penetrates the film, gravity force acts in the downward direction while fluid drag, F_d, surface tension, F_s, and buoyancy force, F_b, oppose particle motion and gradually decelerate the particle. A small amount of impact kinetic energy of the particle is also dissipated due to strain rate established due to fluid flow in the film imparted by the moving particle. The energy spent to overcome the drag force across the film length can be obtained as:

$$E_d = \int_0^{l_f} C_d \left(\frac{\pi}{4}d_p^2\right)\left(\frac{\rho_l v_p^2}{2}\right) dy \qquad (2)$$

where drag coefficient, C_d, for particle immersing in liquid is used as suggested by Wu et al. [14], i.e.:

For $0 < Re \le 1$, $C_d = 24/Re$
For $1 < Re \le 400$, $C_d = 18/Re^{0.646}$
For $400 < Re \le 3 \times 10^5$, $C_d = 0.5$.

While travelling through the film the particle experiences a buoyancy force and energy spent to overcome the net buoyancy force over length of the film that can be expressed as:

$$E_b = \int_0^{l_f} \frac{\pi}{6}d_p^3(\rho_p - \rho_l)g \, dy \ . \qquad (3)$$

The surface tension force remains active only at both top and bottom interfaces and becomes zero when the particle is inside the film. This force prevents motion of the particle as the particle passes through the interfaces. Considering diameter as the characteristic length of the particle, the surface energy spent to completely wet the particle is given by:

$$E_s = 2\pi d_p^2 \sigma . \tag{4}$$

During penetration of the film, local flow is generated in the film due to particle motion which leads to viscous dissipation. Viscous dissipation occurring in the entire process can be expressed [2] as:

$$E_{diss} = \mu_l \int_0^{t_c} \int_0^V \frac{1}{2}\left(\frac{\partial v_i}{\partial x_j} + \frac{\partial v_j}{\partial x_i}\right)^2 dV, \tag{5}$$

where t_c denotes the penetration time, which is defined as contact time duration of the particle with the film. This time can be approximated by the time required to travel across length of the film, $t_c \sim l_f/v_p$, where l_f is the film thickness and v_p is the impact velocity of the particle. Since the particle motion is predominantly in the vertical or y direction, the strain rate terms in the equation of viscous dissipation can be scaled as $\sim u_p/l_f$. The volume to be considered for this viscous dissipation is taken as the volume of the cylindrical shaped film, which is given as $\pi R^2 l_f$. The energy dissipation during the particle motion through the film is therefore:

$$E_{diss} = \mu_l \left(\frac{l_f}{v_p}\right)\frac{1}{2}\left(\frac{v_p}{l_f}\right)^2 \left(\pi R^2 l_f\right). \tag{6}$$

Defining C as the ratio of energy required overcoming all the resistive forces to the impact kinetic energy of the particle, i.e.:

$$C = \frac{E_d + E_b + E_s + E_{diss}}{E_{k0}} . \tag{7}$$

Then after some manipulation, C can be expressed as:

$$C = \frac{1.5 C_d s_{r1}}{\rho_r} + \frac{Ar_p s_{r1}}{\rho_r Re_p^2} + \frac{24}{We_p \rho_r} + \frac{1.5 s_{r2}^2}{\rho_r Re_p}, \tag{8}$$

where S_{r1} is ratio of film thickness to particle diameter, S_{r2} is ratio of particle diameter to film diameter, ρ_r is the density ratio of film and the particle, We is Weber number $\rho_l v_p^2 d_p/\sigma$, Re is Reynolds number $\rho_l v_p d_p/\mu_l$, and Ar is Archimedes number given as $g(\rho_p - \rho_l)d_p^3 \rho_l/\mu_l^2$. The magnitude of C determines the particle-liquid film collision outcomes. If $C>1$, the resistance to penetration is relatively higher and particle is captured in the film. Conversely, when $C\leq1$, the impact inertia of the particle overcomes all resistances in the film and completely penetrates the film.

LIQUID MASS ASSOCIATED WITH PARTICLE

When the particle penetrates the bottom interface a liquid meniscus is formed around the particle surface. The three phase contact line moves up quickly as the particle descends. However, due to adhesion work between the particle surface and the liquid the three phase contact line stops moving further up and a fixed three phase contact line is formed. The meniscus now takes the shape of a liquid ligament which subsequently breaks up creating few satellite droplets. Due to adhesion between the particle surface and liquid a certain amount of liquid remains attached to the particle surface when the ligament breaks off.

Although many studies are available on liquid ligament breakup for cases such as a cylindrical liquid jet and droplet-droplet collision, very less studies [3] are available for ligament breakup during droplet-particle collision. For cylindrical liquid jets two possible mechanisms, capillary wave instability and end pinch-off [12, 13], are known for ligament breakup.

Capillary wave instability arises in the ligament due to small flow perturbations induced by external vibrations which lead to reduction in surface. The process is favoured by surface tension and thus these waves grow further in amplitude. This makes all sinusoidal perturbations with wavelength longer than 2π unstable. In Rayleigh's linear limit, the cylindrical jet is unstable due to natural growth of axisymmetric disturbances. Their growth rate depends on the jet radius and fluid properties.
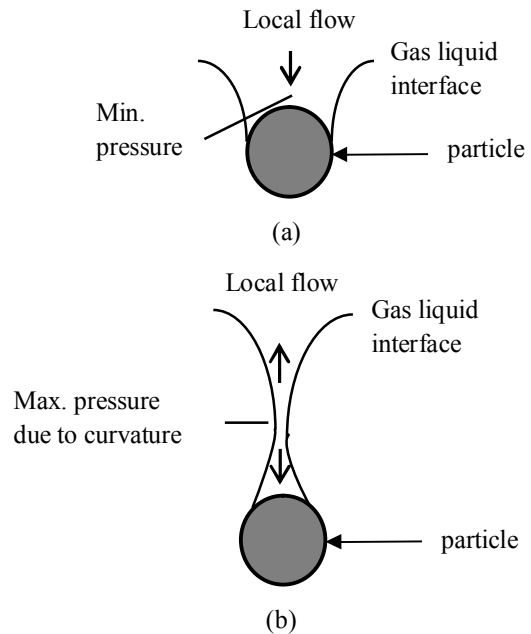
Figure 4 Schematic of ligament breakup by pinching-off mechanism during penetration of liquid film.

For the end pinch-off mechanism the attached liquid ligament gradually elongates and narrows down in the radial direction (Figure 4) due to the continuous downward motion of the particle. When a minimum neck diameter is reached, pressure at this point increases due to curvature of the neck. A non-uniform capillary pressure field propagates along the length of the ligament which subsequently creates a local flow inside the ligament. This flow retracts the ligament in the reverse direction of the particle motion which eventually leads

to pinch off-of the ligament. Stone et al. [12] analysed ligament breakup process during collision of two droplets and they found that the ligament was independently produced through pinching instead of capillary wave instability. It was numerically demonstrated that capillary wave instability leads to ligament break off only for those with higher elongation ratio.

In the present work, at relatively low Weber numbers, it would appear from the experiments that end pinch-off was more likely since the observed elongation ratio of the ligament at rupture was much less than that computed theoretically from capillary wave instability [13]. Hence, pinch-off was assumed for the following energy balance based model to predict the liquid mass remaining with the particle following rupture of the liquid ligament.

Consider a particle impacting on a stationary liquid film as shown in Figure 3. Before impact, the total energy of the system, E_0, comprising the impacting particle and film, is equal to:

$$E_0 = E_{k0} + E_{s0},\qquad(9)$$

where E_{k0} is given by eq. 1, and E_{s0} is the initial surface energy of the film, of flat circular interfaces of diameter, d_f, which can be expressed as:

$$E_{s0} = 2\pi\frac{d_f^2}{4}\sigma.\qquad(10)$$

While penetrating the film the particle kinetic energy is spent on viscous dissipation due to fluid motion and overcoming the resistance from surface tension, buoyancy and drag forces. The sum of these forces, E_1, is equal to:

$$E_1 = E_s + E_d + E_b + E_{diss}.\qquad(11)$$
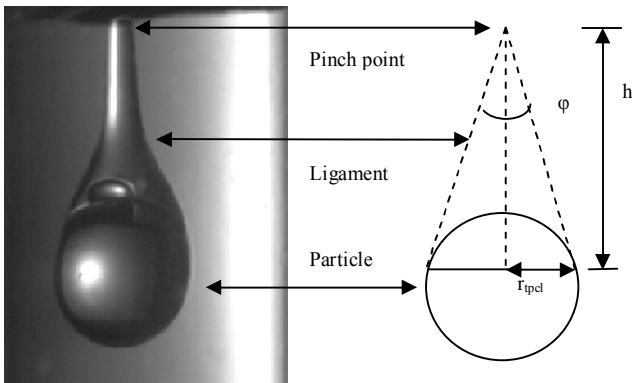
Figure 5 A conical shape volume model of the liquid ligament before breakup is adopted in the present study.

When the particle penetrates the bottom interface, if it still has enough kinetic energy, it will then stretch the bottom meniscus forming a ligament which takes the shape of a cone before the ligament pinches off (see Figure 5). With the aid of high speed imaging it has been confirmed [1] that for self-similar type breakup of ligament an almost constant cone angle,

φ, is invariably obtained before pinch-off. Regardless of the initial shape of the ligament, the cone angle (φ) was reported to be 18.1°.

The surface energy, E_{sl}, due to stretching of the ligament forming a conical part of height, h, and base radius equal to radius of contact line, r_{tpcl}, can be expressed as:

$$E_{sl} = \pi r_{tpcl}\left(\sqrt{h^2 + r_{tpcl}^2}\right)\sigma.\qquad(12)$$

From Figure 3:

$$r_{tpcl} = r_p \sin\psi.\qquad(13)$$

From Figure 5:

$$h = r_{tpcl}\cot\varphi.\qquad(14)$$

Assuming that the entire ligament remains attached to the particle surface no satellite droplets are formed, then the kinetic energy, E_2, of the combined particle and liquid ligament just at the time of pinch-off is given by:

$$E_2 = E_{k1} = \frac{1}{2}(m_p + m_l)v_{p2}^2,\qquad(15)$$

where v_{p2} is the ligament-particle velocity and m_p and m_l are the mass of particle and ligament, respectively. An estimate for v_{p2}, often referred as Taylor-Culick speed, can be obtained, by considering both the acceleration, a_{lig}, and characteristic (capillary) time, t_c, for the ligament breakage. Firstly, t_c is given by [13]:

$$t_c = \sqrt{\frac{\rho_l d_{lig}^3}{\sigma}}.\qquad(16)$$

Secondly, for relatively low Weber numbers, where breakup of the ligament occurs primarily due to pinch-off, a_{lig} can be equated to the ligament inertia (distorting) and surface tension (restoring) forces, i.e.,:

$$\rho_l d_{lig}^3 a_{lig} \sim d_{lig}\sigma,\qquad(17)$$

where d_{lig} is the diameter of the ligament. Hence:

$$a_{lig} = \frac{\sigma}{\rho_l d_{lig}^2}.\qquad(18)$$

Given that velocity is equal to the product of acceleration and time, then from Eqs. (16) and (18) then:

$$v_{p2} = \sqrt{\frac{\sigma}{\rho_l d_{lig}}}.\qquad(19)$$

The unknown in Eq. (19) is d_{lig}, and in practice will vary with time and position during the breakup process. A reasonable approximation is that $d_{lig} \approx 2r_{tpcl}$.

Now the unknown term for liquid mass (m_l) in Eq.15 associated with the particle can be obtained from the geometry of the ligament shown in Figure 5. The mass of liquid (m_l) contained in the cone shaped ligament is volume of the cone times density of the liquid and is expressed as,

$$m_l = \left[\frac{\pi}{3} r_{tpcl}^2 h - \frac{\pi}{3} r_p^3 (2 - cos\psi + cos^3\psi)\right]\rho_l, \qquad (20)$$

where the first and second part of the equation gives the cone volume and spherical cap volume of the particle, respectively. Subsequently, ligament radius (r_{tpcl}) and height (h) can be obtained from Eq. 13 and 14.

The energy balance equation considering total initial energy equals to energy spent to overcome all the resistive forces, formation of the ligament and residual kinetic energy of ligament-particle system, can finally be written as,

$$E_0 = E_1 + E_{sl} + E_2. \qquad (21)$$

Substituting expressions of E_0, E_{sl} and E_2 from Eq. 9, 12 and 15 in Eq. 21, the complete energy balance equation is constituted. The resulting equation has only one unknown variable - penetration angle α which can be solved iteratively to finally obtain liquid mass associated with the particle from Eq. 20.

NUMERICAL METHOD

To simulate the interaction phenomena, a two-phase three dimensional CFD model using interface tracking volume of fluid (VOF) approach was adopted in the finite volume method based commercial CFD solver ANSYS Fluent. The developed 3D model in Cartesian coordinates comprising continuity, momentum and volume fraction equations was solved as follows:

$$\frac{\partial \rho}{\partial t} + \nabla.(\rho \vec{v}) = 0 , \qquad (22)$$

$$\frac{\partial (\rho \vec{v})}{\partial t} + \nabla.(\rho \vec{v}\vec{v}) = -\nabla P + \nabla.[\mu(\nabla \vec{v} + (\nabla \vec{v})^T] + \rho \vec{g} + \vec{F_s}. \quad (23)$$

The mixture density, ρ_{mix}, and viscosity, μ_{mix}, were calculated based on the individual phase fractions, α, where:

$$\rho_{mix} = \rho_l \alpha_l + \rho_g (1 - \alpha_l) , \qquad (24)$$

$$\mu_{mix} = \mu_l \alpha_l + \mu_g (1 - \alpha_l) . \qquad (25)$$

The volume fraction of each dispersed phase was solved by the following advection equation:

$$\frac{\partial \rho_l \alpha_l}{\partial t} + \vec{v}.\nabla \rho_l \alpha_l = 0, \qquad (26)$$

while the phase fraction of the continuous phase was calculated using the following conservation equation:

$$\sum_{i=1}^{n} \alpha_q = 1 . \qquad (27)$$

The momentum equation, in addition to pressure, gravity and viscous stress, included a surface force term, F_s, where:

$$F_s = \sigma \frac{\rho_{mix} \kappa \nabla \alpha_l}{0.5(\rho_l + \rho_v)} . \qquad (28)$$

The curvature of the interface (κ) used in (16) was expressed in terms of surface normal i.e.

$$\kappa = \frac{1}{|n|}\left[\left(\frac{n}{|n|}.\nabla\right)|n| - (\nabla.n)\right]. \qquad (29)$$

The surface normal in the VOF approach is expressed as a gradient of phase volume fraction at the interface and can be written as

$$n = \nabla \alpha_l . \qquad (30)$$

Wall adhesion is significant for fluids with non-zero contact angle on the surface. This effect was incorporated in the model expressing unit normal at the wall boundary in terms of unit vectors $\hat{n}_w$ for fluid and $\hat{t}_w$ for wall and the contact angle (θ) i.e.

$$\hat{n} = \hat{n}_w cos(\theta) + \hat{t}_w sin(\theta) . \qquad (31)$$

A 4.61x12 mm^2 cylindrical geometry with unstructured grid containing 320,256 tetrahedral cells was used for the simulation. For modelling wall adhesion, a static contact angle (θ) of 55° for water on glass particle was applied along with and no-slip boundary conditions. Pressure outlet boundary condition was applied on all the surrounding faces. A second-order upwind scheme was used for discretization of the momentum equation while the volume fraction parameter and pressure were discretized using Geo-Reconstruct and Presto scheme, respectively. Pressure-velocity coupling was obtained by PISO scheme. A residual of 10^{-4} was set for convergence of continuity, momentum and volume fraction equations. All simulations were performed using a time step size of 10^{-6} s with 50 iterations per time step.

To model the solid particle motion, a dynamic meshing technique was used involving smoothing and remeshing scheme on the adjacent cells of the particle boundary. The smoothing scheme involved stretching of cells adjacent to the moving surface using a spring constant based on Hooke's law. A spring constant of 1.0 was used in the present model. When cell motion is large, cells around the moving wall deform heavily and become highly skewed. To avoid simulation failure, these cells required remeshing. For computational efficiency, only the cells which exceeded a specified skewness of 0.7 or a range of cell size (min. to max.) were remeshed. The particle was considered to be a rigid body and motion was obtained by implementing a user defined function based on the six degree of freedom solver. The rotational motion of the particle was not however simulated in the present work.

RESULTS AND DISCUSSIONS

In the experiment, interaction between particle and the film was studied in the Weber number range of 1.4- 23.9. Depending

on the impact Weber number three distinct interaction types were observed. Experimental observations and CFD model predictions at different time instances are presented in Figure 6. Some distinct features of this penetration behaviour can be noticed.
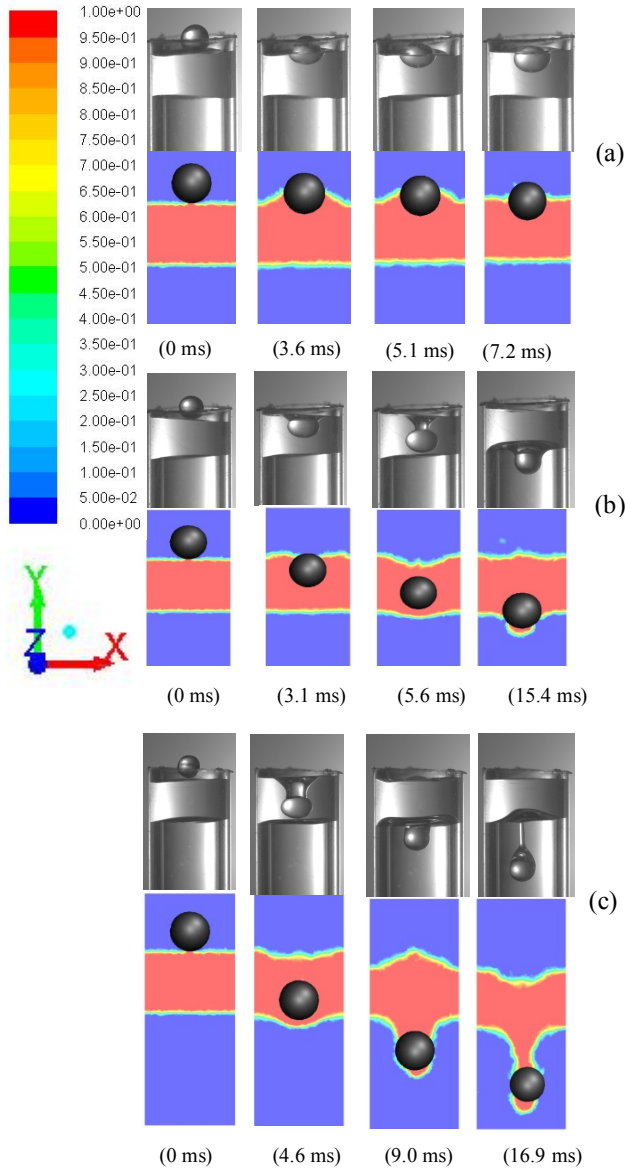

Figure 6 Comparison of experimental observations and CFD modelling predictions of Particle-liquid film interactions behaviour at a) particle penetrates the top interface and remains partially submerged at We-1.4 b) particle penetrates the top interface but gets captured at the bottom interface at We-11.7 and c) particle penetrates the bottom interface and carries finite amount of liquid with it after ligament breakup at We-22.5.

At a low Weber number (We-1.4), as the particle slowly descends, the three phase contact line rises over the particle surface (Figure 6a) and when particle kinetic energy is completely dissipated to overcome the resistive forces, the particle gradually comes to a steady state with decaying amplitude of oscillation at the interface. At an intermediate Weber number (We-11.7), the particle penetrates through the top interface while achieving a partial penetration through the bottom interface. A gas cavity is formed at the top interface which eventually snaps as the radius of three phase contact line gradually diminishes to zero. CFD simulations (Figure 6b) predict an early detachment of the particle but do not predict the observed interface depression very well. This could be attributed to the use of a static contact angle in the model while in reality the contact angle dynamically changes with the velocity of three phase contact line on the particle surface. It should be noted that, the molecular-hydrodynamic contact angle models reported in the literature rely on fitting parameters that are obtained experimentally [8]. Also it is a tedious task to incorporate these dynamic contact angle models into a CFD code. At the bottom interface, further motion of the particle is prohibited by the surface tension force which pulls back the particle in the upward direction causing a rebound at the interface (not shown). The particle then gradually settles down at the bottom interface after few oscillations with decaying amplitude. At higher Weber numbers (e.g. We-22.5), the particle has sufficient kinetic energy to overcome all the resistive forces and penetrates through the film completely (Figure 6c). During penetration of the top interface when the gas cavity collapses, a bubble was observed to attach to the particle surface consistently. The bubble attachment was also observed by Dubrovsky et al. [3] in their studies on droplet-particle collision process at higher impact velocities. A ligament is formed which keeps the particle attached to the bottom interface. The ligament finally pinches off leading to some liquid mass carryover on the particle surface forming a trailing satellite droplet. The CFD simulations however predicted the breakup of the ligament with a slight delay (at 19.5ms, not shown). This could again be attributed to the dynamic nature of the contact angle on particle surface and also inadequate resolution of the ligament interface due to the use of unstructured dynamic mesh which undergoes significant distortions during simulation.

The condition of penetration (*C*) defined by Eq. 8 was used to obtain a regime boundary for the observed particle-film interactions and thus to broadly classify the interactions into two categories – 1) particle captured inside the film and 2) complete penetration of the interface. Figure 7 presents the value of *C* evaluated from Eq. 8 against Weber number. A clear power law dependency of *C* on Weber number can be observed which further simplifies the expression of *C* being dependent on single parameter. In experiments, the particle was observed to be consistently captured at the top and bottom interface for values of C>1 and completely penetrated the film for values of C ≤1. The critical Weber number for complete penetration (C = 1) obtained from the fitted equation was ~ 20 which also agreed well with the experimental observations. Few discrepancies

were however noted where particles were observed to penetrate the film below this critical Weber number which could be attributed to the non-spherical shape of the particle. Interaction outcome in such case depends on the particle shape orientation (relatively sharp or flat face) during impact.
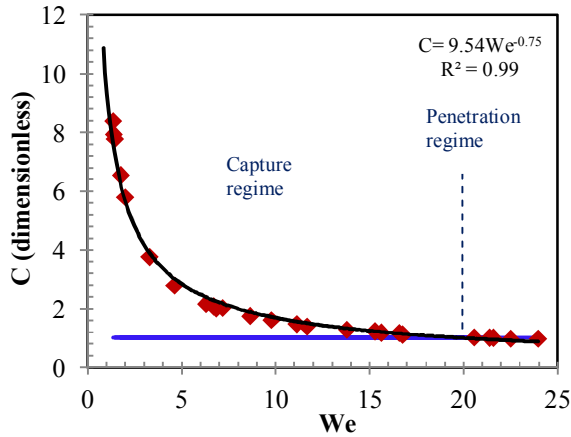

Figure 7 Criterion developed in Eq. based on energy balance approach. Value of C>1 indicates capture of particle in the film while value of C≤1 indicates complete penetration of the film.

It is of interest to look into the particle motion profile during these interactions which brings perspective of different resistive forces which inhibit the particle motion. Figure 8 compares the experimentally obtained particle velocity profile with the CFD model predictions obtained at low to high Weber numbers corresponding to the visuals presented in Figure 6. Figure 8a presents the dynamics at We-1.4, until 7 ms only where the particle has not come to a completely stationary state. The velocity gradually declines as kinetic energy is spent to overcome counteraction of the resistive forces.

In Figure 8b, reversal of the particle velocity is predicted at 11 ms due to rebound off the particle from the bottom interface which as explained before is caused by the surface tension force at the interface. Experimentally however this rebound process was observed late (at ~18 ms) (not shown). The early prediction of CFD model again could be attributed to inability to capture the stretching of meniscus at the bottom interface properly due to use of a static contact angle. In CFD modelling, the meniscus was stretched shorter compared to the experiment which resulted into the model predicting early rebound.

Figure 8c presents the particle motion profile at We of 22.5. Particle penetrates the bottom interface at ~7 ms and then pulls out the bottom meniscus to form the ligament which breaks up at ~18 ms. Interestingly, in this duration, the particle velocity remains almost constant as the ligament keeps expanding at a constant velocity till the breakup. The assumption of using a constant velocity of particle-ligament system in the modelling (Eq.19) of liquid mass carryover is therefore experimentally justified. However, the experimentally obtained particle-ligament system velocity (~0.4 m/s) was higher than the assumed scaled velocity (0.19 m/s) obtained from Eq. 19.
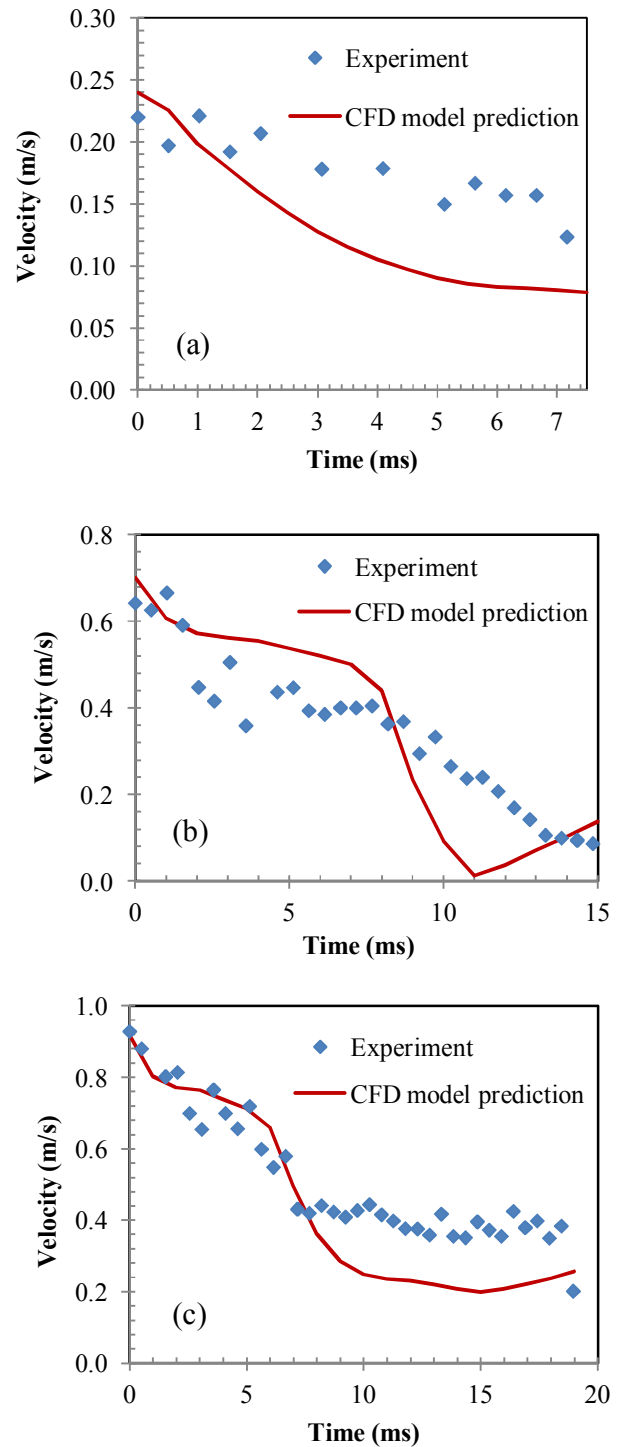
Figure 8 Comparison of experimentally found particle velocity profile and CFD modelling predictions during particle-liquid film interactions at a) We-1.4 b) We-11.7 and c) We-22.5.

The interaction process is governed by the interplay of forces. In CFD modelling, the contributions of all forces are lumped into pressure force (hydrodynamic pressure integrated
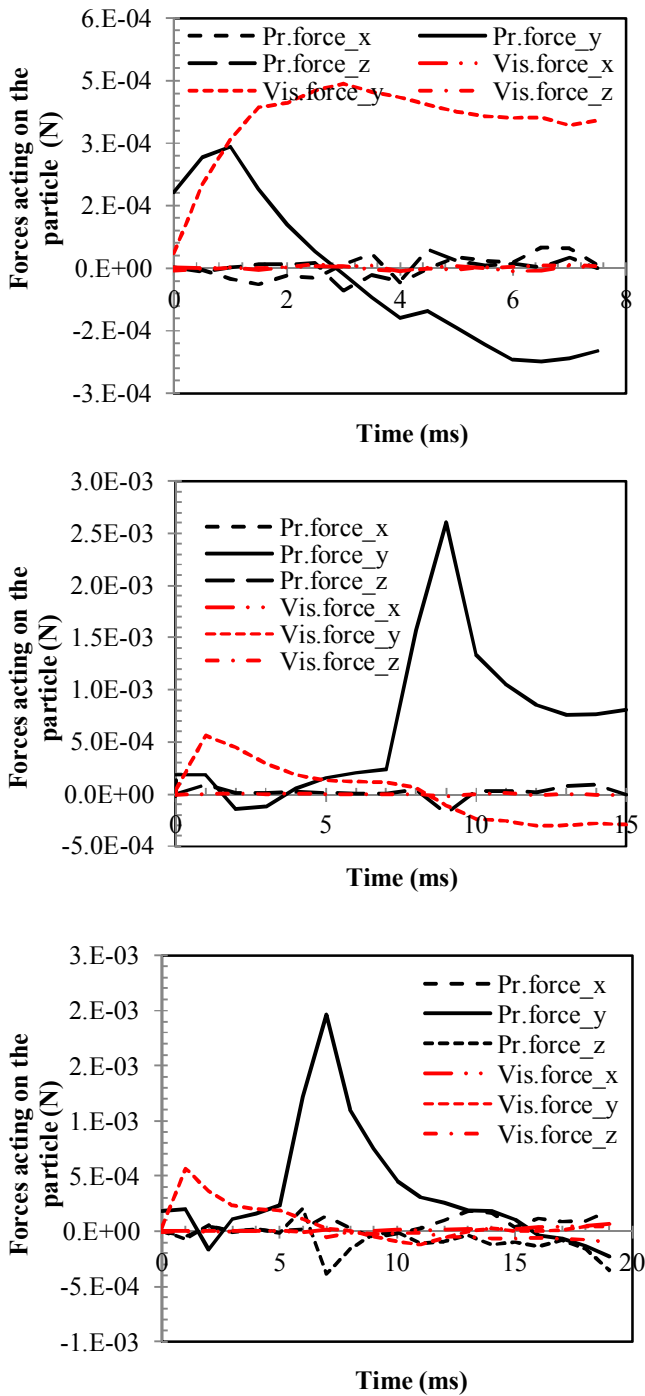
Figure 9 Comparison of pressure and viscous forces in x, y and z directions acting on the particle during the interaction process at a) We-1.4 b) We-11.7 and c) We-22.5. At lower Weber number and pressure force are of same order of same order of magnitude but at higher Weber number, these two forces differ by one order of magnitude.

over particle surface) and viscous force (shear stress integrated

over particle surface). These forces are presented in Figure 9 for three representative Weber numbers.

Due to principally vertical motion of the particle, the y components of the both forces remain dominant over the other components. At low Weber number (We-1.4, Figure 9a), both pressure force and viscous force remain of comparable magnitude, however, at the higher Weber number (Figure 9b-c), the pressure force remains at least a magnitude higher than the viscous force mainly due to a higher impact velocity.

At the higher Weber number, complete penetration of the film was observed where some quantity of the liquid mass always adhered to the particle surface. Due to an adverse pressure gradient established in the ligament (as shown in Figure 4), the ligament finally pinches off forming a satellite droplet.

The model predictions for liquid mass carried by the particle were compared with the experimental measurements (Figure 10).
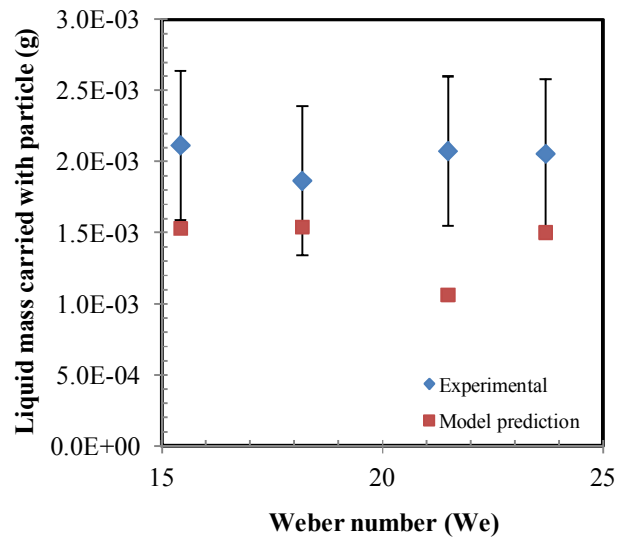

Figure 10 Comparison of liquid mass carryover predicted by the model with experimental measurements.

Experimentally, the interactions of particles with the liquid film were found to be different for the same size particles. The observed deviation is considered to be due to irregularities in the particle shape. Overall, the model predictions were found to be on the lower side of the experimental measurements, but within the uncertainty limits, except for one case. The ligament length before breakup was found to vary in the range of 2.13-3.03mm whilst the model prediction was in the range of 2.26-2.7mm which was fairly close. It is worth noting that two unknown parameters (penetration angle and particle-ligament velocity) in the model were reduced to only one (penetration angle) assuming a constant characteristic velocity which was actually found to be approximately half of the experimentally measured velocity. Additionally, the ligament actually takes shape of a cylindrical strand connected to a smaller cone at the time of detachment which also deviates from the assumed

conical shape of the ligament. Nonetheless, acknowledging the complexities involved in the ligament breakup process, this simplified model can be considered useful to have an analytical estimate of the liquid mass carryover which otherwise is reported empirically [3].

CONCLUSION

In the present work, particle interactions with a confined stationary liquid film were studied at different impact velocities. Broadly two different types of interactions were observed – capture and complete penetration. At Weber numbers < 15, particles were consistently observed to be captured in the film. A critical value of 20 however was theoretically obtained using the condition of penetration developed in the present study which could be attributed to the irregular shape of the particles. At We > 20, the particle was observed to penetrate the film completely carrying out some liquid mass. A liquid ligament trailing behind the particle would finally pinch off forming a small satellite droplet. An analytical model based on end pinch off mechanism of ligament was developed to predict the particle-film interactions and also estimate the liquid mass carryover. The particle-film interactions simulated using the CFD model also agreed well with the experimental observations. However for accurately capturing the phenomena of gas-cavity formation at the top interface and meniscus stretching at the bottom interface, a dynamic contact angle model is indeed required. The role of different forces in the particle-film interactions was analysed using the CFD model which suggests dominance of pressure force over the viscous force at higher impact Weber number cases. To address further complexities involved in the interaction process coupled with heat transfer, as an extension of this work, the future study will focus on the interaction behaviour of hot particles heated above Leidenfrost point with the liquid film gaining a better insight into the industrial applications like FCC vaporization process.

REFERENCES

[1]Castrejon-Pita, J.R. et al., Self-similar breakup of near-inviscid fluids, Physical Review E, 86, 15301(R), 2012, pp. 1-4.

[2]Chandra, S., and Avedisian, C.T., On the collision of a droplet with a solid surface, Proceedings: Mathematical and Physical Sciences, vol. 432, no. 1884, 1991, pp. 13-41.

[3]Dubrovsky, V.V., Podvysotsky, A.M. and Shraiber, A.A., "Particle interaction in three phase polydisperse flows", Int. J. Multiphase Flow, vol. 18, no. 3, 1992, pp. 337-352.

[4] Ge, Y., Fan, L-S., "Droplet-particle collision dynamics with film boiling evaporation", Journal of Fluid Mechanics 573, 2007, pp.311-337.

[5] Hoeven, van der, M.J. "Particle-droplet collisions in spray drying", Ph.D. Thesis, School of Engineering, University of Queensland, Australia, 2008.

[6] Lee, D-G. and Kim, H-Y., "Impact of superhydrophobic sphere onto water", Langmuir, vol. 24, 2008, pp. 142–145.

[7] Lee, D-G., and Kim, H-Y., "Sinking of small sphere at low Reynolds number through interface", Phys. Fluids, vol. 23, 072104, 2011, pp. 1-9.

[8] Liu, D., He, Q., Evans, G.M., "Penetration behaviour of individual hydrophilic particle at a gas-liquid interface", Advanced Particle Processing, vol. 21, 2010, pp. 401-411.

[9] Mitra, S. et al., "Droplet impact dynamics on a spherical particle", Chem. Eng. Sci., vol. 100, 2013, pp. 105-119.

[10] Mitra, S. et al., "Collision behavior of a small spherical droplet on a large stationary droplet", Chemeca, 2013, Brisbane, Qld. Australia.

[11] Nguyen, A.V and Schulze, H.J., "Colloidal science of flotation", Marcel Dekker, Surfactant series, vol. 118, 2004, Chapter 23, pp.527-559.

[12] Stone H.A., Bentley, B.J., and Leal, L.G., An experimental study of transient effects in the breakup of viscous drops, Journal of Fluid Mechanics, vol. 173, 1986, pp. 131-158.

[13] Van Wilm H. et al., Breakup of diminutive Rayleigh jets, *Physics of Fluids,* 22, 122003, 2010, pp. 1-11.

[14] Wu, Y., Zhang, J., and .Lavernia, E.J, "Modelling of the incorporation of ceramic particulates in metallic droplets during spray atomization and coinjection", Metallurgical and Materials Transactions B, vol. 25B, 1994, pp. 135-147.